View metadata, citation and similar papers at core.ac.uk

brought to you by CORE

provided by Archivio istituzionale della ricerca - Alma Mater Studiorum Università di Bologna

This is a post-peer-review, pre-copyedit version of an article published in *Brain Structure and Function*. The final authenticated version is available online at: https://doi.org/10.1007/s00429-017-1369-3

This version is subjected to Springer Nature terms for reuse that can be found at: https://www.springer.com/gp/open-access/authors-rights/aam-terms-v1

THE LAMINAR ORGANIZATION OF THE MOTOR CORTEX IN MONODACTYLOUS MAMMALS. A COMPARATIVE ASSESSMENT BASED ON HORSE, CHIMPANZEE AND MACAQUE

Cozzi B[1]*, De Giorgio A[2,3], Peruffo A[1], Montelli S[1], Panin M[1], Bombardi C[4], Grandis A[4], Pirone A[5], Zambenedetti P[6], Corain L[7], Granato A[2]*.

[1] Department of Comparative Biomedicine and Food Science, University of Padova, Legnaro (PD), Italy
[2] Department of Psychology, Catholic University of the Sacred Heart, Milan (MI), Italy
[3] Faculty of Psychology, eCampus University, Novedrate (CO), Italy
[4] Department of Veterinary Medical Sciences, University of Bologna, Ozzano dell'Emilia (BO), Italy
[5] Department of Veterinary Sciences, University of Pisa, Pisa (PI), Italy
[6] Pathology Division, General Hospital of Dolo-Venezia, Dolo (VE), Italy
[7] Department of Management and Engineering, University of Padova, Vicenza (VI), Italy

* Correspondence to

Bruno Cozzi
Dept. of Comparative Biomedicine and Food Science
University of Padova
Viale dell'Università 16
35020 Legnaro (PD) – Italy
Phone +39.049.8272626
Fax +39.049.8272796
e-mail bruno.cozzi@unipd.it

or

Alberto Granato
Dept. of Psychology
Catholic University of the Sacred Heart
Largo A. Gemelli 1
20123 Milan (MI) – Italy
Phone +39.02.72348588
e-mail alberto.granato@unicatt.it

Abstract

The architecture of the neocortex classically consists of six-layers, based on cytological criteria and on the layout of intra/interlaminar connections. Yet, the comparison of cortical cytoarchitectonic features across different species proves overwhelmingly difficult, due to the lack of a reliable model to analyze the connection patterns of neuronal ensembles forming the different layers.
We first defined a set of suitable morphometric cell features, obtained in digitized Nissl-stained sections of the motor cortex of the horse, chimpanzee, and crab-eating macaque. We then modeled them using a quite general nonparametric data representation model, showing that the assessment of neuronal cell complexity (i.e., how a given cell differs from its neighbors) can be performed by using a suitable measure of statistical dispersion such as the mean absolute deviation – MAD. Along with the nonparametric combination and permutation methodology, application of MAD allowed not only to estimate, but also to compare and rank the motor cortical complexity across different species.
As to the instances presented in this paper, we show that the pyramidal layers of the motor cortex of the horse are far more irregular than those of primates. This feature seems could be related to the different organization of the motor system in monodactylous mammals.

Key Words: motor cortex; horse; chimpanzee; crab-eating macaque; mean absolute deviation

Introduction

The order Perissodactyla includes mammals (equines, rhinos, tapirs) that underwent extreme evolutionary specialization of the distal bony components of the limb, reduced to a major metacarpal bone (with two accessory thin side metacarpals) and a single digit, whose distal phalanx is encased in the hoof. The reduction of the distal segments functional to rapid locomotion in vast open spaces, together with the necessary limits in lateral rotation movements of the wrist, brought also a general decrease of reciprocal mobility of the segments of the forearm, restricted only to dorso-ventral flexion-extension movements. Consequently, the general muscle organization of the distal forelimb of Perissodactyla is much simpler than that of the five-fingered, supination/pronation able primates, and the motor control is also presumably less complex.

The whole central control of the single-finger hand has never been studied in detail, and a modern neuroanatomy of Ungulates (including odd- and even-toed mammals) does not exist (Nieuwenhuys et al. 1998). Although the horse possesses a relatively heavy brain of approx. 600 g (Cozzi et al. 2014), with considerable cortical folding (Zilles et al. 2013) details on the organization of its cortex received little to no attention. The lack of interest in these herbivores may be obviously due to the difficulty of studying large bodies, and to the moral, ethical, and practical impossibility of performing experimental and invasive procedures. However, the control of a single-fingered hand, capable only of flexion movements due to the lack of supination/pronation in the forearm, has a potential relevance for comparative studies and for the precise understanding of how the motor control of the hand shapes the wiring of the brain and its general organization in different mammalian orders. Simplification of forelimb mechanics is accompanied by the need for precise synchronization of the movements of the four limbs, and requires motor scheme generators in the brainstem, as in general true for quadrupeds (Musienko et al. 2014). The currently accepted concept of cortico-spinal connections in Ungulates suggests predominance of polysynaptic (= extrapyramidal) pathways (for general outline see Seiferle 1975). There is a general consensus that regulation of the limb movements in the large herbivores is mostly due to the rubro-spinal, tecto-spinal, vestibulo-spinal and reticulo-spinal pathways (Barone, 1966; Chiocchetti et al. 2006; Grandis et al. 2007), while direct monosynaptic (= pyramidal) pathways are mostly limited to regulation of head and proximal neck movements.

The motor cortex of the large herbivores received scarce attention. The organization of the cortical column in primates and rodents has the classical six-layered structure with the regional variations described in details ever since the classical early maps of Brodmann (1909). On the contrary, the laminar organization of hoofed animals - at least in even-toed terrestrial Cetartiodactyla (including among the others the bovine and the swine) - shows the prevalence of a five-layer structure, with extreme reduction of layer 4 (inner granules), generally considered to be directly activated by the thalamus for sensory inputs (Constantinople and Bruno 2013). Differences in the cytoarchitectonics are reflected by a different neurochemical organization of the cortical column: Studies involving the presence, concentration and distribution of calcium-binding proteins in Cetartiodactyla indicate that parvalbumin (PV), a marker of thalamo-recipient granules (Martin del Campo et al 2014), is reduced or absent in these species. A partial exception is the visual cortex in which PV is easily recognized. The amino-acid sequence of PV is somewhat different in Ungulates (including Perissodactyla and terrestrial and marine Cetartiodactyla) with respect to Primates, thus partially explaining the observed discrepancies in presence and distribution. However, even given the possibility of an incorrect immunocytochemical identification of the protein due to different amino-acid sequence and faulty recognition in tissue samples, the columnar organization of hoofed herbivores remains clearly different, and presumably suggests that different modalities of circuitries are operating.

In the present study we compared the cortical organization of the motor cortex of the horse, the most common Perissodactyla, with that of two primates, the crab-eating macaque and the chimpanzee. We are aware of the limits of a study of layer thickness and neural density. To this effect we devised a new experimental analytic technology for this specific purpose, to gain a further insight into the nature of neural

cells that constitute the cortical column of the motor cortex of representative species of the two orders. As a direct indicator we used MAD (Mean Absolute Deviation) that allows the analysis of single neurons with complex multi-variables. Thus, our study does not analyze neuron size or shape variation (irregularity), but rather their inherent complexity, that is, their tendency to be similar (or not) to the surrounding neurons comprised within a defined spatial unit in the cortical column.

Materials and methods

Animal tissue

For the present study we used samples from different mammals. The species and details are summarized in Table 1. The chimpanzees were housed in a local zoo-safari facility. Their bodies and those of the three horses were delivered to the necropsy room of the Department of Comparative Biomedicine and Food Science of the University of Padova for post-mortem diagnostic procedures. Under these circumstances, no ethic permission is required as the animals were not part of any experiment. All the causes of death revealed absence of neuropathology.

The three crab-eating macaques were brought to the necropsy room indicated above for post-mortem following euthanasia at the end of a translational xenotransplant experiment authorized by the Ethical Committee and the Italian Ministry of Health. The Authors of the present study were not involved in the xenotransplant procedures and had nothing to do with the said experiment. The brains of the crab-eating macaques were stored in the archives of the same Department and then used for the present investigation. Use of archival samples is encouraged based on the EU Directive 2010/63/ of 22 September 2010 on the protection of animals used for scientific purposes (Introduction section #27)[1].

Brains from the different species were fixed by immersion in buffered formalin. The time interval between death and removal of the brain of the chimpanzee # 36675 cannot be determined precisely, as the animal was found dead by the wardens on the morning round. Chimpanzee # 64361 died during urgent surgical procedures due to a gastrointestinal disorder. The brains of the crab-eating macaques were removed within one hour after sacrifice. Time intervals between death and brain removal for the horses varied between two and twelve hours.

Localization of motor cortex and sampling procedures

Identification of the motor cortex of the hand in the three primate species was based on commonly available atlases (Delucchi et al. 1965; Paxinos et al. 1999). The motor cortex of the finger of horse was identified based on the position relative to the cruciate sulcus and on the available literature (Ramón y Cajal 1917; Breazile et al. 1966).

Histology

Tissue blocks of nervous tissue were fixed by immersion in buffered formalin, washed in phosphate-buffered saline (PBS) 0.1 M, pH 7.4 and processed for paraffin embedding. Archival samples from the crab-eating macaques were extensively washed in PBS before paraffin embedding. Tissue samples were cut into 4µm thick sections.

Computerized analysis of the Nissl sections

Quantitative cytoarchitectonic features were examined in sections from the crab-eating macaques, chimpanzees and horses, by using an automated procedure. Briefly, microphotographs of representative Nissl-stained coronal sections of the motor cortex (Fig. 1A) were thresholded using the automatic gating algorithm of ImageJ software (http://rsb.info.nih.gov/ij/) (Fig. 1B). The medio-lateral width of the analyzed regions of interest (ROIs) was 1-1.2mm. The mean thickness of the ROIs (from the pial surface to the subcortical white matter) was 2,211µm for the horse, 2,387µm for the chimpanzee, and 2,624µm for the macaque. The ROI were subdivided into 19 continuously adjoining frames, located at different dorso-ventral depths (the height of each stripe was 110-140µm). Within each frame, for all the cell profiles with area greater than 25µm^2, the following parameters were calculated using the "Analyze" menu of ImageJ: area, perimeter, shape descriptors (Fig. 1C) (see below). Data acquisition was controlled by custom macros written in the ImageJ Macro Language.

[1] "Member States should, where appropriate, facilitate the establishment of programmes for sharing the organs and tissue of animals that are killed".

Although excluding particles smaller than 25µm^2, the present analytical method does not allow us to discriminate between small neurons and large glia cells. For the present study we will define the identified cells as "neurons", but we are aware of the possible inclusion in the category of an undefined number of large glial cells.

Immunohistochemistry

Immunohistochemical analysis was performed in sections from the crab-eating macaques, chimpanzees and horses as follows. Formalin-fixed-paraffin-embedded (FFPE) tissues were sectioned at a thickness of 4µm and stained using the Ventana automated immunostainer BenchMark XT (Ventana Medical Systems, Tucson, AZ, USA). The slides were dried at 60 °C for 1 hour and deparaffinized using EZ Prep (Ventana Medical Systems) at 75 °C for 4 minutes. We used the following antibodies: mouse monoclonal anti-PV (1:5000, Swant Inc), mouse monoclonal anti-calretinin (CR) (1:2000, Swant Inc), rabbit policlonal anti-CR (1:2000, Swant Inc), mouse monoclonal anti-calbindin (CB) (1:5000, Swant Inc), rabbit policlonal anti-CB (1:10.000, Swant Inc).

Cell conditioning was performed using CC1 solution (Ventana Medical Systems) at 100 °C for 32 minutes. Signals were detected using UltraView DAB IHC Detection Kit (Ventana Medical Systems). Counterstaining was performed with Hematoxylin for 4 min at room temperature.

Statistical analysis

Morphometric features definition

As neural cell morphometric features we used a set of four variables belonging to two related domains, i.e. size and irregularity:

1. *P*=Perimeter, i.e. the total length of neural cell boundary measured in micron;
2. *LA*=Linear Area, defined as $LA = \sqrt{4\pi \cdot Area}$; *LA* is actually a linear measure expressed in micron; note that, in case of perfect circumference, $LA = \sqrt{4\pi \cdot \pi \cdot radius^2} = 2\pi \cdot radius = P$;
3. *AR*=Aspect Ratio, defined as $AR = major\ axis\ /\ minor\ axis$;
4. *LI*=Linear Irregularity, defined as $LI = P\ /LA$.

It is worth noting that *P* and *LA* are size measures conforming to the rule "the larger they are, the larger is the neuron dimensionality"; both features are measured in micron. The last two variables *AR* and *LI* are shape-based measures conforming to the rule "the larger they are, the larger is the neuron irregularity"; both features are measured as dimensionless ratios. Also note that *AR*≥1, *LI*≥1 and *LI*=*AR*=1 only in the case of a perfect circumference.

Neural cell morphometry modelling

From the statistical point of view, it is worth noting that the two issues of complexity characterization of motor cortex neural cells and their related inter-species comparisons are actually complex multivariate problems where the depth of the cortical column needs also to be taken into account. In this regard, we adopted a fully nonparametric approach which allows us to avoid the explicit specification neither of any given reference random distribution nor of the functional form of the multivariate morphological response. This statistical approach, that is suitable for complex morphometric analysis, has been proposed by (Montelli et al 2016), focusing on the variations of the dendritic branching pattern of granule neurons in the presence (or absence) of exogenous estradiol administration.

To formally address the problem, let us assume without loss of generality that the *p*-dimensional morphometric features **Y** of the *i*-th neural cell from the *j*-th species located in the *l*-th cortex layer can be modelled as

$$\mathbf{Y}_{ij}(l) = \boldsymbol{\mu} + \boldsymbol{\eta}_j(l) + \boldsymbol{\varepsilon}_{ij}(l), \qquad (1)$$

where $\boldsymbol{\varepsilon}_{ij}(l)$ are i.i.d. non-Gaussian error terms with null mean and scale coefficients $\boldsymbol{\sigma}^2_j(l)=\boldsymbol{\sigma}(\boldsymbol{\eta}_j(l))$ and unknown distribution $P_{\boldsymbol{\varepsilon}}$, $\boldsymbol{\mu}$ is a population constant, coefficients $\boldsymbol{\eta}_j(l)$ represent the *main effects* and may depend on layer through any kind of function, but are independent of units and $\boldsymbol{\sigma}(\boldsymbol{\eta}_j(l))$ are layer-varying scale coefficients which may depend, through monotonic functions, on main treatment effects $\boldsymbol{\eta}_j$.

Since is well known that many neuronal cell types may be simultaneously present within one layer of motor cortex, it is advisable to generalize model (1) and refer to a more flexible and realistic mixture distribution model (McLachlan and Peel 2004). This approach is recommended by the literature when the information regarding the reference subpopulation from which the sample has been drawn is unavailable; such is our case, where the class to which each examined neuronal cell belongs is unknown. Without loss of generality assume that there are G type of neuronal cells (i.e. granules, pyramidal cells, etc.) whose unknown proportions in the *l*-th cortex layer are represented by parameters $\pi_j(l)$, j=1,…,G. Within this framework, it can be easily demonstrated that mean and variance of $\mathbf{Y}_{ij}(l)$ are

$$\mathbb{E}[\mathbf{Y}ij(l)]=\boldsymbol{\mu}_j(l)=\boldsymbol{\mu}+\Sigma_g \pi_j(l)\cdot_g\boldsymbol{\eta}_j(l), \qquad (2)$$

$$V[\mathbf{Y}_{ij}(l)]=\boldsymbol{\sigma}^2_j(l)=\Sigma_g \pi_j(l)[(\boldsymbol{\eta}_j(l)-\boldsymbol{\mu}_j(l))^2+\boldsymbol{\sigma}^2_j(l)]. \qquad (3)$$

It is worth noting that the inference on $\boldsymbol{\sigma}^2_j(l)$ is strongly related to the concept of neural cell complexity, i.e. the higher or lower probability to observe, within a given layer, a large cell variation in its morphometric features.

Complexity statistic and composite indicators

The *complexity* of neural cells from cortical column can be viewed as the multidimensional morphological propensity to observe, within a given layer, a large variation in neuronal sizes and shapes. With reference of our data representation model (1), an investigation on complexity means performing inference on $\boldsymbol{\sigma}^2_j(l)$ scale parameters as in expression (3).

To quantitatively estimate the complexity, a suitable univariate scatter-based statistic is needed. To this aim, we selected a suitable univariate scatter statistic such as the mean absolute deviation – *MAD* (Pham-Gia and Hung 2001)

$$MAD_{jk}(l) = \frac{1}{n_j(l)}\sum_{i=1}^{n_j(l)}|y_{ijk}(l) - \bar{y}_{ijk}(l)|,\ j=1,...,C,\ k=1,...,p,\ l=1,...,L, \qquad (4)$$

where $\bar{y}_{jk}(l) = \frac{1}{n_j(l)}\sum_{i=1}^{n_j(l)} y_{ijk}(l)$ represents the sample mean.

Note that as scatter statistic we do not use the sample standard deviation. In fact, the *MAD* statistic offers three main advantages: (i) it can be considered as a more robust indicator to infer on variability in case of non-Gaussian distributions (Habib El Amir 2012); (ii) since the practical meaning of the standard deviation remains unclear, *MAD* has been proposed to be used in place of standard deviation because it offers a direct measure of the data dispersion (Pham-Gia and Hung 2001); (iii) when used as test statistic within the permutation and combination framework, *MAD* has more suitable properties than the sample standard deviation (Pesarin and Salmaso 2010). Note that, even if defined at layer level, the *MAD* is actually an individual cell-based quantity measuring the tendency of a neuron to be more or less similar to the neurons that are located in its proximity.

Multivariate hypothesis testing and ranking on complexity

We shortly present below a nonparametric permutation and combination-based approach to perform multivariate hypothesis testing and ranking on neuronal cell complexity. The proposed method is an extension to multivariate scatter problems of the multivariate location testing (Corain and Salmaso 2004; Pesarin and Salmaso 2010) and ranking problems (Corain and Salmaso 2007; Arboretti et al. 2014; Corain et al. 2016).

Let us assume that data are drawn from *C* multivariate populations $\Pi_1,...,\Pi_C$ (i.e. species), *C*>2, by means of a sampling procedure, so allowing inference on their possible equality and, in case this hypothesis is rejected, to rank these populations in order to obtain a relative rankings from the 'large' to the 'small' ones according to pre-specified meaningful criteria.

With reference to the data representation model (1) presented in the first sub-section, let us formalize the problem within a nonparametric framework: let **Y** be the continuous *p*-dimensional response variable represented as a *p*-vector of the observed data from population Π and let us assume without loss of generality that more scattered values of each univariate aspect *Y* correspond to a larger marginal scatter-

feature, so that when comparing two populations the possible marginal stochastic dispersion dominance of one population over the other should result in a higher ranking position.

We emphasize that our goal is to classify and ranking $\Pi_1,\ldots,\Pi_C$ multivariate populations with respect to p marginal variables when C samples $\mathbf{Y}_1,..,\mathbf{Y}_C$ are drawn from C populations, where n_j is the number of observations, $j=1,\ldots,C$. More formally, we are looking for an estimate of the rank ${}_{scat}r(\Pi_j(l))$, i.e. the relative scatter stochastic orderings of each population when compared among all other populations, i.e. more formally

$$ {}_{scat}r(\Pi_j(l))=1+\sum_{j\neq h} I\left(I\left(\mathbf{Y}_j(l) \overset{d,scat}{<} \mathbf{Y}_h(l)\right)\right)=1+\{\#\, I\left(\mathbf{Y}_j(l) \overset{d,scat}{<} \mathbf{Y}_h(l)\right),\ h=1,\ldots,C,\ j\neq h\},\ j=1,\ldots,C, \tag{5} $$

where $I(\cdot)$ is the indicator function and # means the number of times. Note that definition (5) is derived by using the concept of stochastic dominance and pairwise counting how many populations are scatter-based stochastically larger than that a specific population (for more details see Arboretti et al. 2014 and Corain et al. 2016).

Under the hypothesis $H_0(l)$ of scatter distributional equality of all the C populations, all true ranks would necessarily be equal to one, hence they would be defining a full ex-aequo situation, that is

$$ {}_{scat}r(\Pi_j(l)\,|\,H_0(l))=\{1+\#\left(\mathbf{Y}_j(l) \overset{d,scat}{<} \mathbf{Y}_h(l)\right),\ h=1,\ldots,C,\ j\neq h\}=1,\ \forall\, j. $$

This situation of equal ranking where all populations belong to a single scatter ranking class may be formally represented in a hypotheses testing framework where the hypotheses of interest are:

$$ \begin{cases} H_0(l): \mathbf{Y}_1(l) \overset{d,scat}{=} \cdots \overset{d,scat}{=} \mathbf{Y}_C(l) \equiv \boldsymbol{\sigma}_1^2(l) = \cdots = \boldsymbol{\sigma}_C^2(l) \\ H_1(l): \exists \mathbf{Y}_j(l) \overset{d,scat}{\neq} \mathbf{Y}_h(l) \equiv \exists \boldsymbol{\sigma}_j^2(l) \neq \boldsymbol{\sigma}_h^2(l), j,h=1,\ldots,C, j\neq h \end{cases} \tag{6} $$

In case of rejection of the global multivariate hypothesis $H_0(l)$, that is, when data are evidence that at least one population behaves differently from the others, it is of interest to perform inferences on pairwise comparisons between populations, i.e.

$$ \begin{cases} H_{0(jh)}(l): \mathbf{Y}_j(l) \overset{d,scat}{=} \mathbf{Y}_h(l) \equiv \boldsymbol{\sigma}_j^2(l) = \boldsymbol{\sigma}_h^2(l) \\ H_{1(jh)}(l): \left[\left(\mathbf{Y}_j(l) \overset{d,scat}{<} \mathbf{Y}_h(l)\right) \cup \left(\mathbf{Y}_j(l) \overset{d,scat}{>} \mathbf{Y}_h(l)\right)\right] \\ \qquad\qquad \equiv \left[\left(\boldsymbol{\sigma}_j^2(l) < \boldsymbol{\sigma}_h^2(l)\right) \cup \left(\boldsymbol{\sigma}_j^2(l) > \boldsymbol{\sigma}_h^2(l)\right)\right] \end{cases} . \tag{7} $$

To provide suitable, and possibly corrected by multiplicity p-values, the permutation and combination-based approach proposed by Pesarin and Salmaso (2010) can be effectively applied for properly solving the scatter testing problem in (7) and at the same time for ranking the C multivariate populations by estimating their ranks ${}_{scat}r(\Pi_j(l))$ (for details see Corain et al. 2016).

Results

Anatomical description of the motor cortex
The identification of the primate motor cortex was based on atlases for the crab-eating macaque, and the chimpanzee (Delucchi et al. 1965; Paxinos et al. 1999). The cortex of the chimpanzee was especially similar to the human motor cortex although the whole size of the gyri was smaller and the area consequently reduced. Identification of the motor cortex of the horse was based on the presence of the cruciate sulcus whose shortness and extremely anterior position required utmost attention and critical evaluation of available maps of the cortical sulci and gyri.

Conventional histology and computer analysis of the columns
The structure and organization were similar in two primate species, and in the horse. Nissl analysis showed different organization of the cortical column between primates and horse.

Primates - The motor cortex showed the typical presence of six cell layers according to the well described classical model. The motor cortex of the chimpanzee and crab-eating macaque presented vivid staining and a clearly recognizable laminar organization.

Horse - The horse cortex showed clear indication of a layered organization and was easily analyzed.

Immunohistochemistry of calcium-binding proteins
The observed differential expression of calcium binding proteins (Fig. 2) emphasized the different laminar organization of the motor cortex in the two groups.

Calbindin (Fig. 2, top row)
Primates - The motor cortices of the chimpanzee (Fig. 2A) and crab-eating macaque (Fig. 2B) were very similar and showed a fine and dense network of Calbindin-immunoreactive (CB-ir) cells. Specifically, many relatively small neurons were present in the outer layers, and larger CB-ir elements were clearly identified in correspondence to the apparent layers 4-5.
Horse - CB-ir cells were clearly evident in the motor cortex of the horse (Fig. 2C), but their density, and staining intensity were different from those of the two primate species. The CB-ir neurons were present in the outer layers, but the density and intensity of stain of elements in the deeper layers were less evident than in the two primates.

Calretinin (Fig. 2, middle row)
Primates - The Calretinin-immunoreactive (CR-ir) cells were mostly concentrated in the top layers of the chimpanzee (Fig. 2D) and crab-eating macaque (Fig. 2E), although several well evident neurons were present also in the apparent layers 4-5.
Horse - Staining for CR was very scarce in the horse cortex (Fig. 2F), and limited to a few CR-ir neurons in the middle of the cortical column.

Parvalbumin (Fig. 2, bottom row)
Primates - PV stain revealed numerous positive (PV-ir) cells in all the layers of the motor cortex in both the chimpanzee (Fig. 2G) and crab-eating macaque (Fig. 2H).
Horse - Staining for PV was very rare in the horse (Fig. 2I).

Neural density
We have examined the density of neural cells by calculating the percentage of the area of each frame occupied by cellular elements (Fig. 3A) or by obtaining the cell packing density (Fig. 3B) using conventional Nissl-stained slides.

Using both systems the cellular density of the chimpanzee was consistently higher than in the macaque and horse, although some of the deeper frames of the macaque (see frame 16) showed a density comparable to that of the corresponding frames of the chimpanzee. We also emphasize that the computer-assisted evaluation of density indicates a rather important reduction in the percentage of area occupied by cells x surface of the frame (Fig. 3A) for frames 10-12 of the chimpanzee, although this variation is not evident when the sections are observed under the microscope.

Analysis of shape-based features (linear area and perimeter variation, mean values and MAD)
The combined approach allowed a combined analysis of intra- and inter-species variation and variability of linear area (Fig. 3C) and perimeter (Fig. 3D) of all neurons that are comprised within the same frame. The general shape of the variability of linear area (Fig. 3C) shows that the parameters in the three species are relatively similar, notwithstanding different values for both sample mean and MAD. On the other hand, the perimeter of the neurons of the three species (Fig. 3D) indicates marked variations between both primates and the horse especially in correspondence to frames 10-13 (approx. in the middle of the fifth layer), where the cells of the horse exhibited increasing perimeters.

Analysis of irregularity-based features (aspect ratio and linear irregularity mean and MAD)
Macaque and chimpanzee show a similar profile of aspect ratio (Fig. 3E), meaning that cells have a similar disposition of the internal diameters except for frames 10 (corresponding to the top of layer 5) and 15 (corresponding to the bottom of layer 5), respectively, where the chimpanzee cells show a peak. The results thus suggest that most of the primate cells have near spherical shape in both species (except for frames 10 and 15 from the chimpanzee). Both species have very similar profile also for linear irregularity (Fig. 3F), meaning that cells are basically similar and again present relatively regular shapes. In the horse, frames 10 to 16 (upper layer 5 to top of layer 6) present a definitely diverse profile for aspect ratio (Fig. 3E). Differences from the two primates are evident especially for linear irregularity (Fig. 3F), where frames 8-13 from the horse indicate extreme irregularity of shape of the neural cells.

Global neural size
Analysis of global neural size synthesizes the parameters examined above and their representation into a single graph that considers functional layers as obtained in the former analyses. The data confirm that the chimpanzee motor cortex contains larger neurons, but the general trend of dimensional variation is comparable among the three species. The horse is the species in which the irregularity of the neural shape is more pronounced, while the two primates have very similar trends and relatively regular shape of the neural cells. The Fig. 4A confirms the data showing that the chimpanzee has larger neurons with the same complexity of the macaque. The motor cortex of the horse contains relatively large and medium sized but very irregular neurons (Fig. 4B). Overall our data indicate that the differences in the organization of the motor cortex between the two primate species and the horse appear quite marked.

Discussion

The primary motor cortex of primates (area 4) is considered an “agranular” cortex, in which layer 4 is absent in postnatal life (for review see Geyer et al. 2011). However, recent studies performed in adult Rhesus monkeys (García-Cabezas and Barbas 2014), using SMI-32 as a neural marker, described the presence of distinct interneurons, corresponding to those of layer 4 present in other “granular” areas. We emphasize these results here, as all the cerebral cortex of all Ungulates was described as “five-layered” or agranular in previous seminal papers (Hof et al. 1999, 2000), and the presence or absence of a distinct layer 4 could be of paramount importance in a comparative assessment between a 5-layered and a 6-layered cortex. Studies performed in hoofed Cetartiodactyla (pig, kudu, springbok, and giraffe) established that there is no significant variation in the number of neurons in the isocortex of these closely phylogenetically related species (Kazu et al. 2014, 2015). However, the NeuN-based methodology used does not necessarily labels the same populations of neurons across a broad range of mammals (Charvet et al. 2016). Thus, new tools are required to perform in-depth comparisons, and the analysis of comparatively poorly studied but large-brained species may greatly contribute to knowledge of the evolution of the cortex (Charvet et al. 2016).

Our study is focused on the motor cortex, and identification of the hand motor cortex of primates presents little or no difficulty, based on reference atlases (Delucchi et al. 1965; Paxinos et al. 1999). Pioneer stimulation experiments (Breazile et al. 1966) and anatomical studies (Barone 1959) performed in the horse indicated that an area adjacent to the cruciate sulcus is responsible for motor control of specific body parts. Consequently, we identified the motor cortex responsible for the single hoofed finger of the horse based on the topography of the cruciate sulcus, although physiological support for the correspondence is rather limited. The general disposition of the sulci and gyri in the cortex of the horse and other Perissodactyla is remarkably complex (Breazile et al. 1966; Haarmann 1974; Zilles et al. 2013), and a degree of uncertainty is therefore difficult to avoid when attempting inter-order comparisons. Moreover, given the paucity of references (see Johnson 1990), a distinction between a primary motor (= area 4) and a supplementary motor (= area 6) cortex in the horse was impossible at sampling. Since present day ethical and practical problems hamper the possibility to perform electrophysiological experiments on the horse (and other large herbivores) to unravel cortical control of hand movements as performed in primates (see Brown and Teskey 2014 and Schaffelhofer et al. 2015 for recent elegant studies), novel physiological support to morphological hypotheses will be difficult to obtain.

Observation of the Nissl-stained slides of presumed hand motor cortex of the horse showed an apparent prevalence of pyramidal neurons and a low cellular density in comparison to both primates. In fact, instrumental data indicate that the area occupied by neurons is larger in the chimpanzee than in the macaque and horse (Fig. 3A), and that, furthermore, the cell density is also higher (Fig. 3B). The higher cellular density in the brain of the ape possibly reflects the complexity of the circuitry, but the higher values, observed especially in frames 11-15 (Fig. 3B) may also be explained by the different organization of the cortico-spinal tract (CST) between primates and horse. The primate hand-relative CST includes crossed fibers bound to synapses in the cervico-thoracic enlargement that gives rise to the brachial plexus. According to lesion studies (Barone 1959; Verhaart 1962), or to the general relationship between the extension of the pyramidal tract and digital dexterity (Heiffner and Masterton 1975), the CST in the horse is considered to be mostly limited to the brainstem, where descending fibers synapse with generator of motor schemes nuclei that will form the origin of descending polysynaptic tracts. Central pattern generators are specific for a peculiar gait, and in the horse their functional output may be influenced by gene mutations (Katz 2016). However relatively old but elegant electrophysiological investigations involving direct stimulation of the pyramids and recording in the radial and tibial nerve of the horse evidenced the existence of an extended CST in this species, even if the conduction velocities recorded were inferior to those of primates (Breazile et al. 1967), although the diameters of the fibers are apparently in the same range (Towe 1973). Although the question cannot be settled based on the literature or our data, we note here that the distance the fibers have to travel may also influence the size and density of motor neurons.

The distribution of the three calcium-binding proteins examined indicates that CR and PV are not widely expressed in the cerebral cortex of the horse, and that CB is the only protein in this group with an apparent density and distribution comparable to those observed in primates. Our data support the conclusion of previous studies on calcium-binding proteins performed in Cetartiodactyla (Hof et al. 1999, 2000), an Order of mammals that includes other large – but even-toed - herbivores. In primates and rodents PV-ir neurons include relatively large basket-type neurons and chandelier-type neurons, with a prevalent distribution in layer 3 and in thalamo-recipient layer 4. The relative scarcity of PV-ir (and CR-ir) elements that we noted in the horse implies a different organization of the cortical circuitry from that described in rodents and primates (Godlove et al. 2014). In fact, calcium-binding protein topography suggests that Perissodactyla may have developed a peculiar organization of the cortical columns with a certain similitude to what has been described in terrestrial and marine Cetartiodactyla. The comparative reduction or total lack of layer 4 in Cetartiodactyla (Morgane et al. 1988; Hof et al. 1999, 2000) and Perissodactyla may be due to the migration of thalamo-recipient neurons to the upper layers 1 and 2. Consequently, the organization of the local cortical microcircuits may follow the recently proposed organization for agranular cortices (Beul and Hilgetag 2015).

Stereological methods may greatly improve the intra-specific definition of cortical areas (Schleicher et al. 2000; Henssen et al. 2016), but are difficult to apply in comparative neuroscience. Functional comparison of human and monkey cortical areas is based on a number of well-defined categorizations based on the similitudes in hand structure and mobility, but become hypothetical when applied to rodents (for recent review see Orban 2016). To this effect, recent mathematical approaches proposed an unequivocal definition of the neuronal soma for morphometric analysis (Luengo-Sanchez et al. 2015). To address some of the open questions on the general organization of the motor cortex of Perissodactyla, here we propose a statistical method to examine, quantify and - up to a certain extent - qualify the neurons in the cortical column. Our MAD approach may help to define how similar a neuron is with respect to surrounding neurons, and consequently to allow subdividing the thickness of the cortex of a species not only into layers, but into zones of similar morphology and functional significance, thus solving e.g. the problem of relatively ubiquitous pyramidal neurons.
Analysis of the linear area confirms that the basal organization of the cortex in the three species is similar (Fig. 3C), but also indicates that the neurons of the chimpanzee have higher values. However, neurons in frames 9-13 (approx. corresponding to layer 5) of the horse are far more irregular (Fig. 3F) than in primates, or that their shape is more distant from a spherical one (i.e., most of them are pyramidal). So the chimpanzee has larger neurons (Fig. 4A), but the horse possesses a higher quantity of relatively large and irregular neurons (Fig. 4B), and therefore possibly more basket cells or more of the large pyramidal neurons concentrated in a smaller area.
In all mammals studied so far, neuronal density decreases with increasing number and size of the neurons, except in primates (Herculano-Houzel et al. 2014). Recent comparative studies performed in the mouse and Rhesus monkey suggest that pyramidal neurons of equivalent size in a given layer (i.e. layer 3) may greatly differ between the two species in dendritic length, branching patterns, electrophysiological properties and other parameters between species (Gilman et al. 2016). We are also aware of the potential effect of age on dendritic branching and morphology, as described in the chimpanzee and human (Bianchi et al. 2013). In our experimental settings, frames 10-16 (approx. corresponding to layer 5) contain Betz cells. Betz cells are more than conventional pyramidal cells of gigantic size, in that they differ from the general model by showing numerous dendrites originating from the whole circumference of the soma (Geyer et al. 2011). The complex dendritic arborization of Betz cells is hard to identify in Nissl-stained preparations, but may be the reason for a higher MAD expression in the cortex of the horse. The existence of large, irregular pyramidal neurons in non-primate species is well documented, and in a recent study, three species of wild African rodents (*Thryonomys swinderianus*, *Tatera branstii*, and *Rhabdomys pumilio*) were shown to display larger, more branched and more spinous pyramidal neurons than primates (including macaque and baboon) in V1 area (Elston and Manger 2014).

According to the currently prevailing opinions on the organization of the motor system in the horse (Seiferle 1975; Barone and Bortolami 2004), the majority of pyramidal cells of layer 5 are supposedly directed to the brainstem where they synapse with the motor nucleus of the facial nerve or other nuclei (tegmental nuclei, reticular formation, red nucleus, inferior olivary nucleus, vestibular nuclei) responsible for the motor schemes essential for quadrupedal locomotion. However, the elegant data of Breazile et al. (1967) indicate that at least some of the pyramidal cells of the motor cortex of the horse are organized into a true CST tract with smaller fibers that persist till the lumbo-sacral plexus. Such an organization would involve the co-existence of two sets of pyramidal cells, projecting to the generators of motor schemes in the brainstem, and to the spinal cord, respectively. Although such projections also exist in primates, their respective consistence is different in the horse: brainstem-bound fibers would potentially include the majority of neurons, but true CST projections must be considered too. In this mixed organization of the projecting system the dimensions of the pyramidal neurons of the horse could vary greatly, as indeed we noted in our results. Here we also emphasize that the absolute size of the brain (approx. 600 g. for the horse; 400 g for chimpanzee; and 90 g. for the crab-eating macaque) may also explain some minor differences in neuronal size.

Our data suggest that the motor cortex of apes and monkeys is characterized by the presence of a relatively higher numbers of round-shaped neurons (granule cells), especially in the supragranular layers and that the sizes of neighboring cells are highly heterogeneous (i.e., the MAD and the complexity are higher). That cognitive functions are sustained by the great variety of cortical interneurons was already recognized by Ramón y Cajal (1917). However, whether is more convenient for the cerebral cortex to have spatially clustered cells with similar morpho-functional attributes, or adjacent neurons showing non-homogeneous features, is still a matter of debate. For instance, GABAergic interneurons clustered in the 3D space are more effective in tuning the properties of their synaptically targeted pyramidal neurons (Ebina et al. 2014). Moreover, cortical interneurons belonging to the same functional type, but not to different categories, are interconnected through gap junctions (Galarreta and Hestrin 1999; Gibson et al. 1999) and some of these networks are of pivotal importance for the generation of cortical oscillations (Cardin et al. 2009). On the other hand, the diversity of cortical interneurons is thought to be an advantage in terms of cortical computation. Modeling studies suggest that the variance in an interneuronal population can strongly influence the network behavior (Aradi and Soltesz 2002). Consistent with this view, our data point out that some layers of the motor cortex in highly convoluted mammals are characterized by a high heterogeneity of neuronal types (mainly interneurons) and suggest a new set of statistical parameters to compare the cortical cytoarchitetonics across different species. Our data also strongly point to the composite nature of the cortical layers in the horse, with neurons of variable size and irregular shape especially in layer 5, a potential support to the hypothesized co-existence of projections to either the brainstem or the spinal cord in proportions different than in primates**.**

Acknowledgements
The present study has been sponsored by Grants from the University of Padova to BC, AP, LC. The Authors would like to thank Dr. Sandro Mazzariol for the performing the post-mortem on the chimpanzees and horses, and Dr. Giuseppe Palmisano and Dr. Michele Povinelli for help in sampling the tissues, all from the Dept. of Comparative Biomedicine and Food Science of the University of Padova. The Authors also wish to thank Maria Rosa Pittarello from the “Pietro Arduino” Library of the University of Padova at Legnaro (PD) for her precious help in tracing old literature.

References

Aradi I, Soltesz I (2002) Modulation of network behaviour by changes in variance in interneuronal properties. J Physiol (Lond) 538:227-251. doi:10.1113/jphysiol.2001.013054

Arboretti GR, Bonnini S, Corain L, Salmaso L (2014) A Permutation Approach for Ranking of Multivariate Populations. J Multivar Anal 132:39-57. doi:10.1016/j.jmva.2014.07.009

Barone R (1959) Observations sur le faisceau pyramidal des équidés. Bull Soc Sci Vet Med Comp Lyon 5:265-271

Barone R (1966) Observations sur le faisceau rubro-spinal des équidés. C.R. Assoc Anat 131:115-121

Barone R, Bortolami R (2004) Anatomie comparée des mammifères domestiques. 6/1 Système Nerveux Central. Vigot, Paris

Beul SF, Hilgetag CC (2015). Front Neuroanat 8:165. doi:10.3389/fnana.2014.00165

Bianchi S, Stimpson CD, Duka T, Larsen MD, Janssen WGM, Collins Z, Bauernfeind AL, Schapiro SJ, Baze WB, McArthur MJ, Hopkins WD, Wildman DE, Lipovich L, Kuzawa CW, Jacobs B, Hof PR, Sherwood CC (2013) Synaptogenesis and development of pyramidal neuron dendritic morphology in the chimpanzee neocortex resembles humans. Proc Natl Acad Sci USA 110(suppl 2):10395-10401. doi:10.1073/pnas.1301224110

Breazile JE, Jennings DP, Swafford BC (1967) Conduction velocities in the corticospinal tract of the horse. Exp Neurol 17:357-363

Breazile JE, Swafford BC, Biles DR (1966) Motor cortex of the horse. Am J Vet Res 27:1605-1609

Brodmann K (1909) Localisation in the cerebral cortex. Smith-Gordon, London

Brown AR, Teskey GC (2014) Motor cortex is functionally organized as a set of spatially distinct representations for complex movements. J Neurosci 34:13574-13585. doi:10.1523/jneurosci.2500-14.2014

Cardin JA, Carlén M, Meletis K, Knoblich U, Zhang F, Deisseroth K, Tsai LH, Moore CI (2009) Driving fast-spiking cells induces gamma rhythm and controls sensory responses. Nature 459:663-667. doi:10.1038/nature08002

Charvet CJ, Reep RL, Finlay BL (2016) Evolution of cytoarchitectural landscapes in the mammalian isocortex: Sirenians (*Trichechus manatus*) in comparison with other mammals. J Comp Neurol 524:772-782. doi:10.1002/cne.23864

Chiocchetti R, Bombardi C, Grandis A, Mazzuoli G, Gentile A, Pisoni L, Joechler M, Lucchi ML (2006) Cytoarchitecture, morphology and lumbosacral spinal cord projections of the cattle red nucleus. Am J Vet Res 67:1662-1669. doi:10.2460/ajvr.67.10.1662

Constantinople CM, Bruno RM (2013) Deep cortical layers are activated directly by thalamus. Science 340:1591-1594. doi:10.1126/science.1236425

Corain L, Arboretti R, Bonnini S (2016) Ranking of Multivariate Populations - A Permutation Approach with Applications. CRC press, Boca Raton

Corain L, Salmaso L (2004) Multivariate and Multistrata Nonparametric Tests: the NonParametric Combination method. J Mod App Stat Meth 3:443-461

Corain L, Salmaso L (2007) A nonparametric method for defining a global preference ranking of industrial products. J Appl Stat 34:203-216. doi:10.1080/02664760600995122

Cozzi B, Povinelli M, Ballarin C, Granato A (2014) The brain of the horse: weight and cephalization quotients. Brain Behav Evol 83:9-16. doi:10.1159/000356527

Delucchi MR, Dennis BJ, Adey WR (1965) A stereotaxic atlas of the chimpanzee brain (*Pan satyrus*). University of California Press, Berkeley

Ebina T, Sohya K, Imayoshi I, Yin ST, Kimura R, Yanagawa Y, Kameda H, Hioki H, Kaneko T, Tsumoto T (2014) 3D clustering of GABAergic neurons enhances inhibitory actions on excitatory neurons in the mouse visual cortex. Cell Rep 9:1896-1907. doi:10.1016/j.celrep.2014.10.057

Elston GN, Manger PR (2014) Pyramidal cells in V1 of African rodents are bigger, more branched and more spiny than those in primates. Front Neuroanat 8:4. doi:10.3389/fnana.2014.00004

Galarreta M, Hestrin S (1999) A network of fast-spiking cells in the neocortex connected by electrical synapses. Nature. 402:72-75. doi:10.1038/47029

García-Cabezas MA, Barbas H (2014) Area 4 has layer IV in adult primates. Eur J Neurosci. 39:1824-1834. doi:10.1111/ejn.12585

Geyer S, Luppino G, Rozzi S (2011) Motor cortex. In: Mai JK, Paxinos G (eds) The human nervous system, 3rd edn. Academic Press, Amsterdam, pp 1012-1035

Gibson JR, Beierlein M, Connors BW (1999) Two networks of electrically coupled inhibitory neurons in neocortex. Nature. 402:75-79. doi:10.1038/47035

Gilman JP, Medalla M, Luebke JI (2016) Area-specific features of pyramidal neurons - A comparative study in mouse and Rhesus monkey. Cereb Cortex. doi:10.1093/cercor/bhw062

Godlove DC, Maier A, Woodman GF, Schall JD (2014) Microcircuitry of agranular frontal cortex: testing the generality of the canonical cortical microcircuit. J Neurosci 34:5355-5369. doi:10.1523/jneurosci.5127-13.2014

Grandis A, Bombardi C, Travostini B, Gentile A, Joechler M, Pisoni L, Chiocchetti R (2007) Vestibular nuclear complex in cattle: Topography, morphology, cytoarchitecture and lumbo-sacral projections. J Vestib Res 17:9-24

Haarmann K (1974) Morphologische und histologische untersuchungen am neocortex einiger Perissodactyla. Acta Anat (Basel) 90:285-299

Habib El Amir EA (2012) On uses of mean absolute deviation: decomposition, skewness and correlation coefficients. Metron 70:145-164

Heiffner R, Masterton B (1975) Variation in form of the pyramidal tract and its relationship to digital dexterity. Brain Behav Evol 12:161-200

Henssen A, Zilles K, Palomero-Gallagher N, Schleicher A, Mohlberg H, Gerboga F, Eickhoff SB, Bludau S, Amunts K (2016) Cytoarchitecture and probability maps of the human medial orbitofrontal cortex. Cortex 75:87-112. doi:10.1016/j.cortex.2015.11.006

Herculano-Houzel S, Manger P, Kaas JH (2014) Brain scaling in mammalian evolution as a consequence of concerted and mosaic changes in numbers of neurons and average cell size. Front Neuroanat 8:77. doi:10.3389/fnana.2014.00077

Hof PR, Glezer II, Condé F, Flagg RA, Rubin MB, Nimchinsky EA, Vogt Weisenhorn DM (1999) Cellular distribution of the calcium-binding proteins parvalbumin, calbindin, and calretinin in the neocortex of mammals: phylogenetic and developmental patterns. J Chem Neuroanat 16:77-116. doi:10.1016/S0891-0618(98)00065-9

Hof PR, Glezer II, Nimchinsky EA, Erwin JM (2000) Neurochemical and cellular specializations in the mammalian neocortex reflect phylogenetic relationships: evidence from primates, cetaceans, and artiodactyls. Brain Behav Evol 55:300-310

Johnson JI (1990) Comparative development of somatic sensory cortex. In: Jones EG & Peters A (eds) Cerebral Cortex, vol 8B. Comparative structure and evolution of cerebral cortex, part II. Plenum Press, New York, pp 335-449

Katz PS (2016) Evolution of central pattern generators and rhythmic behaviours. Philos Trans R Soc Lond B Biol Sci 371:20150057. doi:10.1098/rstb.2015.0057

Kazu RS, Maldonado J, Mota B, Manger PR, Herculano-Houzel S (2014) Cellular scaling rules for the brain of Artiodactyla include a highly folded cortex with few neurons. Front Neuroanat 8:128. doi:10.3389/fnana.2014.00128

Kazu RS, Maldonado J, Mota B, Manger PR, Herculano-Houzel S (2015) Corrigendum: Cellular scaling rules for the brain of Artiodactyla include a highly folded cortex with few neurons. Front Neuroanat 9:39. doi:10.3389/fnana.2015.00039

Luengo-Sanchez S, Bielza C, Benavides-Piccione R, Fernaud-Espinosa I, DeFelipe J, Larrañaga P (2015) A univocal definition of the neuronal soma morphology using Gaussian mixture models. Front Neuroanat 9:137. doi:10.3389/fnana.2015.00137

Martin del Campo H, Measor K, Razak KA (2014) Parvalbumin and Calbindin expression in parallel thalamocortical pathways in a gleaning bat, *Antrozous pallidus*. J Comp Neurol 522:2431-2445. doi:10.1002/cne.23541

McLachlan G, Peel D (2004) Finite Mixture Models. John Wiley & Sons, New York

Montelli S, Suman M, Corain L, Cozzi B, Peruffo A (2016) Sexually diergic trophic effects of estradiol exposure on developing bovine cerebellar granule cells. Neuroendocrinology. doi:10.1159/000444528

Morgane PJ, Glezer II, Jacobs MS (1988) Visual cortex of the dolphin: An image analysis study. J Comp Neurol 273:3-25

Musienko PE, Deliagina TG, Gerasimenko YP, Orlovsky GN, Zelenin PV (2014) Limb and trunk mechanisms for balance control during locomotion in quadrupeds. J Neurosci 34:5704-5716. doi:10.1523/jneurosci.4663-13.2014

Nieuwenhuys R, ten Donkelaar HJ, Nicholson C (1998) The central nervous system of vertebrates, vol 3. Springer-Verlag, Heidelberg, p 1640

Orban GA (2016) Functional definitions of parietal areas in human and non-human primates. Proc Biol Sci 283:20160118. doi:10.1098/rspb.2016.0118

Paxinos G, Huang X-F, Toga AW (1999) The rhesus monkey brain in stereotaxic coordinates. Academic Press, San Diego

Pesarin F, Salmaso L (2010) Permutation tests for complex data-theory and software. Wiley, Chichester

Pham-Gia T, Hung TL (2001) The Mean and Median Absolute Deviations. Math Comput Model 34:921-936. doi:10.1016/S0895-7177(01)00109-1

Ramón y Cajal S (1917). Recuerdos de mi vida. Tomo II, Historia de mi labor científica. Imprenta y Librería de Nicolás Moya, Madrid

Schaffelhofer S, Agudelo-Toro A, Scherberger H (2015) Decoding a wide range of hand configurations from macaque motor, premotor, and parietal cortices. J Neurosci 35:1068-1081. doi:10.1523/jneurosci.3594-14.2015

Schleicher A, Amunts K, Geyer S, Kowalski T, Schormann T, Palomero-Gallagher N, Zilles K (2000) A stereological approach to human cortical architecture: identification and delineation of cortical areas. J Chem Neuroanat 20:31-47. doi:10.1016/S0891-0618(00)00076-4

Seiferle E (1975) Nervensystem. In: Nickel R, Schummer A, Seiferle E (eds) Lehrbuch der anatomie der haustiere, vol 4. Verlag Paul Parey, Berlin und Hamburg, pp 3-188

Towe AL (1973) Relative numbers of pyramidal tract neurons in mammals of different sizes. Brain Behav Evol 7:1-17

Verhaart WJC (1962) The pyramidal tract. Its structure and functions in man and animals. World Neurol 3:43-53

Zilles K, Palomero-Gallagher N, Amunts K (2013) Development of cortical folding during evolution and ontogeny. Trends Neurosci 36:275-284. doi:10.1016/j.tins.2013.01.006

Figure captions

Fig. 1 Schematic representation of the acquisition process and subsequent transformation of the image into a set of data. **A** - Nissl image of the motor cortex of the crab-eating macaque; **B** - ImageJ threshold rendering of A; **C** - schematic representation of data relative to Frames 1 - 3 (out of 19). Data relative to area and perimeter are expressed in µm or μm^2, respectively (1 μm^2 = 1 pixel); data on aspect ratio are a-dimensional. Scale bar = 200µm

Fig. 2 Immunocytochemistry of calcium binding proteins in the three species. Top row, Calbindin (CB); middle row, Calretinin (CR); bottom row, Parvalbumin (PV). Note the different (much lower) density for CR- and PV-ir neurons in the horse. Scale bars: A-C and G-I = 500µm; D-F = 200µm

Fig. 3 A - Neuron density defined as the ratio between the sum of area covered by neurons divided by the whole frame surface. Neuron density was calculated within each frame and for all species where *Equus caballus*, *Macaca fascicularis* and *Pan troglodytes* are represented by blue, red and green solid line respectively. **B -** Neuron count density defined as the ratio between the total number of neurons found in each 10,000 square micron. Neuron count density was calculated within each frame and for all species where *Equus caballus*, *Macaca fascicularis* and *Pan troglodytes* are represented by blue, red and green solid line respectively. **C -** Sample mean (upper solid lines, vertical axis on the left) and MAD-Mean Absolute Deviation (lower dashed lines, vertical axis on the right) of linear area defined as $\sqrt{4\pi \cdot neuron\ area}$. Mean and MAD of linear area were calculated from all neurons observed within each frame and for all species where *Equus caballus*, *Macaca fascicularis* and *Pan troglodytes* are represented by blue, red and green solid line respectively. One or two stars and crosses mean respectively a single or double significance dominance of one figure when compared with the other two figures, where a significant dominance of f1 over f2 means that the null hypothesis f1=f2 was rejected at the 5% significance level in favour of H1: f1>f2. Raw permutation p-values were used to possible reject H0 vs. H1 (without any type of correction by multiplicity). Cortical columns of each specie were superimposed in the figure along with the numbering of related layers. **D** - Sample mean (upper solid lines, vertical axis on the left) and MAD- Mean Absolute Deviation (lower dashed lines, vertical axis on the right) of neuron perimeter. Mean and MAD of perimeter were calculated from all neurons observed within each frame and for all species where *Equus caballus*, *Macaca fascicularis* and *Pan troglodytes* are represented by blue, red and green solid line respectively. One or two stars and crosses mean respectively a single or double significance dominance of one figure when compared with the other two figures, where a significant dominance of f1 over f2 means that the null hypothesis f1=f2 was rejected at the 5% significance level in favour of H1: f1>f2. Raw permutation p-values were used to possible reject H0 vs. H1 (without any type of correction by multiplicity). Cortical columns of each specie were superimposed in the figure along with the numbering of related layers. **E -** Sample mean (upper solid lines, vertical axis on the left) and MAD- Mean Absolute Deviation (lower dashed lines, vertical axis on the right) of neuron aspect ratio defined as the ratio between the major and the minor neuron axes. Mean and MAD of aspect ratio were calculated from all neurons observed within each frame and for all species where *Equus caballus*, *Macaca fascicularis* and *Pan troglodytes* are represented by blue, red and green solid line respectively. One or two stars and crosses mean respectively a single or double significance dominance of one figure when compared with the other two figures, where a significant dominance of f1 over f2 means that the null hypothesis f1=f2 was rejected at the 5% significance level in favour of H1: f1>f2. Raw permutation p-values were used to possible reject H0 vs. H1 (without any type of correction by multiplicity). Cortical columns of each specie were superimposed in the figure along with the numbering of related layers. **F -** Sample mean (upper solid lines, vertical axis on the left) and MAD- Mean Absolute Deviation (lower dashed lines, vertical axis on the right) of linear irregularity defined as the ratio between perimeter and linear area. Mean and MAD of linear irregularity were calculated from all neurons observed within each frame and for all species where *Equus caballus*, *Macaca fascicularis* and *Pan troglodytes* are represented by blue, red and green solid line respectively. One or two stars and crosses mean respectively

a single or double significance dominance of one figure when compared with the other two figures, where a significant dominance of f1 over f2 means that the null hypothesis f1=f2 was rejected at the 5% significance level in favour of H1: f1>f2. Raw permutation p-values were used to possible reject H0 vs. H1 (without any type of correction by multiplicity). Cortical columns of each specie were superimposed in the figure along with the numbering of related layers

Fig. 4 A - Scatter plot of global mean in size (average of linear area and perimeter) vs. global mean in irregularity (average of aspect ratio and linear irregularity). Each dot was calculated within each frame and for all species where *Equus caballus*, *Macaca fascicularis* and *Pan troglodytes* are represented by blue, red and green dots respectively. Ranking analysis results, separately for size and irregularity features, are superimposed in the figure where the inequality "<" means that a significant dominance in mean of one specie over one other was observed, that is the null hypothesis specie1=specie2 was rejected at the 5% significance level in favour of H1: specie1>specie2. Adjusted multivariate permutation p-values (i.e. corrected by multiplicity) were used to possible reject H0 vs. H1. **B** - Scatter plot of global MAD in size (average of linear area and perimeter) vs. global MAD in irregularity (average of aspect ratio and linear irregularity). Each dot was calculated within each frame and for all species where *Equus caballus*, *Macaca fascicularis* and *Pan troglodytes* are represented by blue, red and green dots respectively. Ranking analysis results, separately for size and irregularity features, are superimposed in the figure where the inequality "<" means that a significant dominance in scatter of one specie over one other was observed, that is the null hypothesis specie1=specie2 was rejected at the 5% significance level in favour of H1: specie1>specie2. Adjusted multivariate permutation p-values (i.e. corrected by multiplicity) were used to possible reject H0 vs. H1

Figure 1

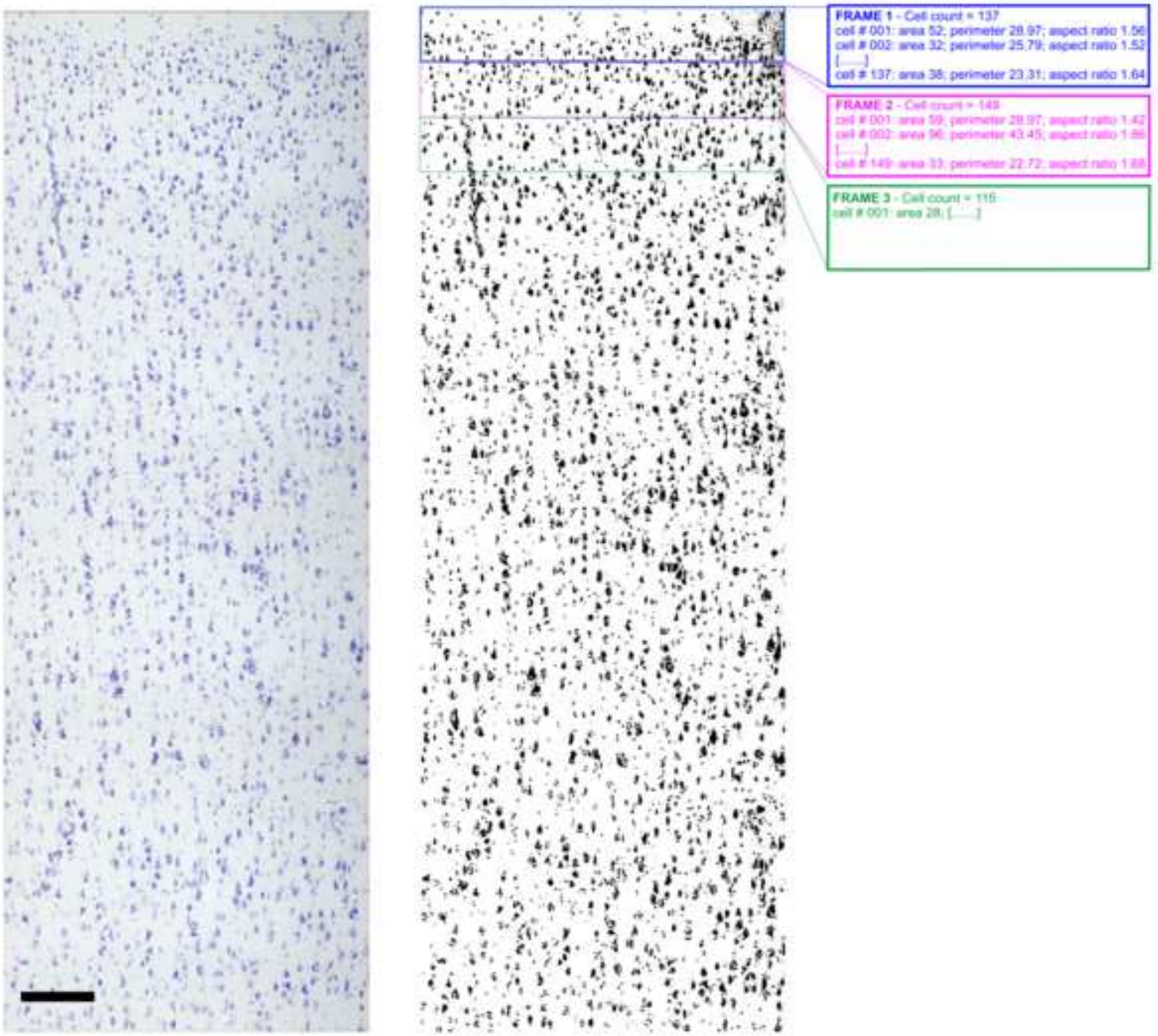
FRAME 1 - Cell count = 137
cell # 001: area 52; perimeter 28.97; aspect ratio 1.56
cell # 002: area 32; perimeter 25.79; aspect ratio 1.53
[.....]
cell # 137: area 38; perimeter 23.31; aspect ratio 1.64
FRAME 2 - Cell count = 149
cell # 001: area 59; perimeter 28.97; aspect ratio 1.42
cell # 002: area 96; perimeter 43.45; aspect ratio 1.66
[.....]
cell # 149: area 33; perimeter 22.72; aspect ratio 1.68
FRAME 3 - Cell count = 115
cell # 001: area 28; [.....]

Figure 2

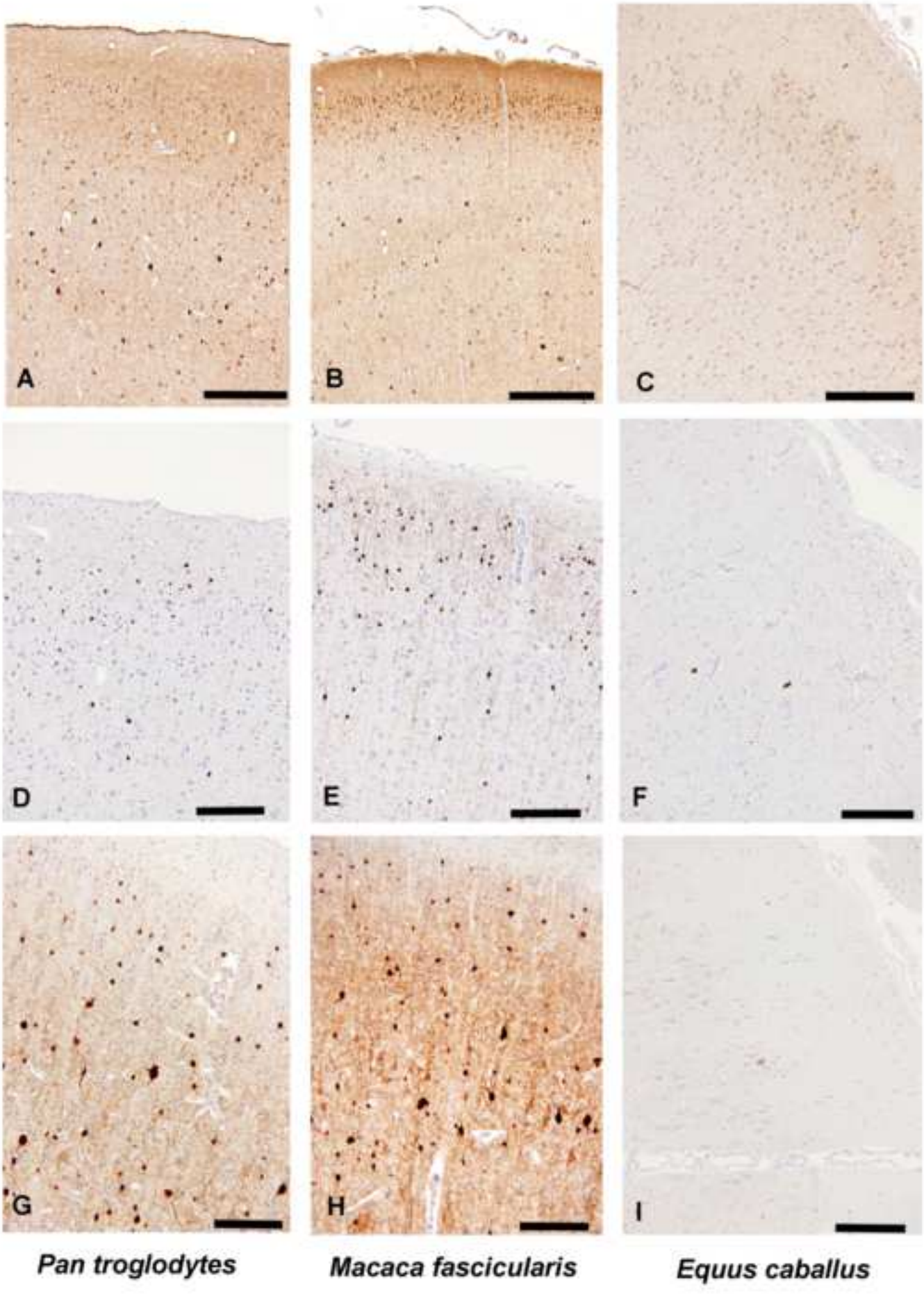
A
B
C
D
E
F
G
H
I
Pan troglodytes
Macaca fascicularis
Equus caballus

Figure 3

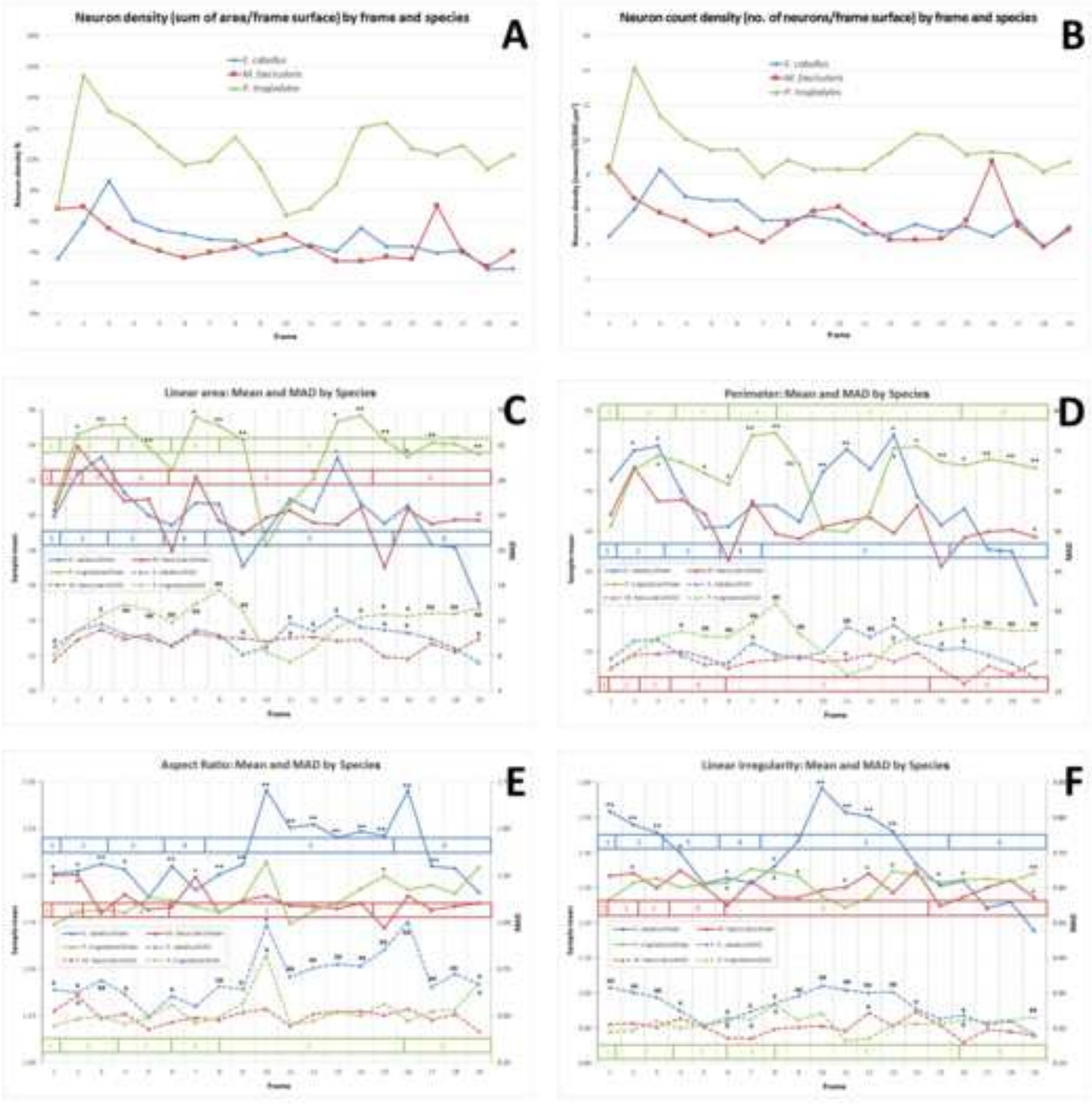
Neuron density (sum of area/frame surface) by frame and species
A
Neuron count density (no. of neurons/frame surface) by frame and species
B
Linear area: Mean and MAD by Species
C
Perimeter: Mean and MAD by Species
D
Aspect Ratio: Mean and MAD by Species
E
Linear irregularity: Mean and MAD by Species
F

Figure 4

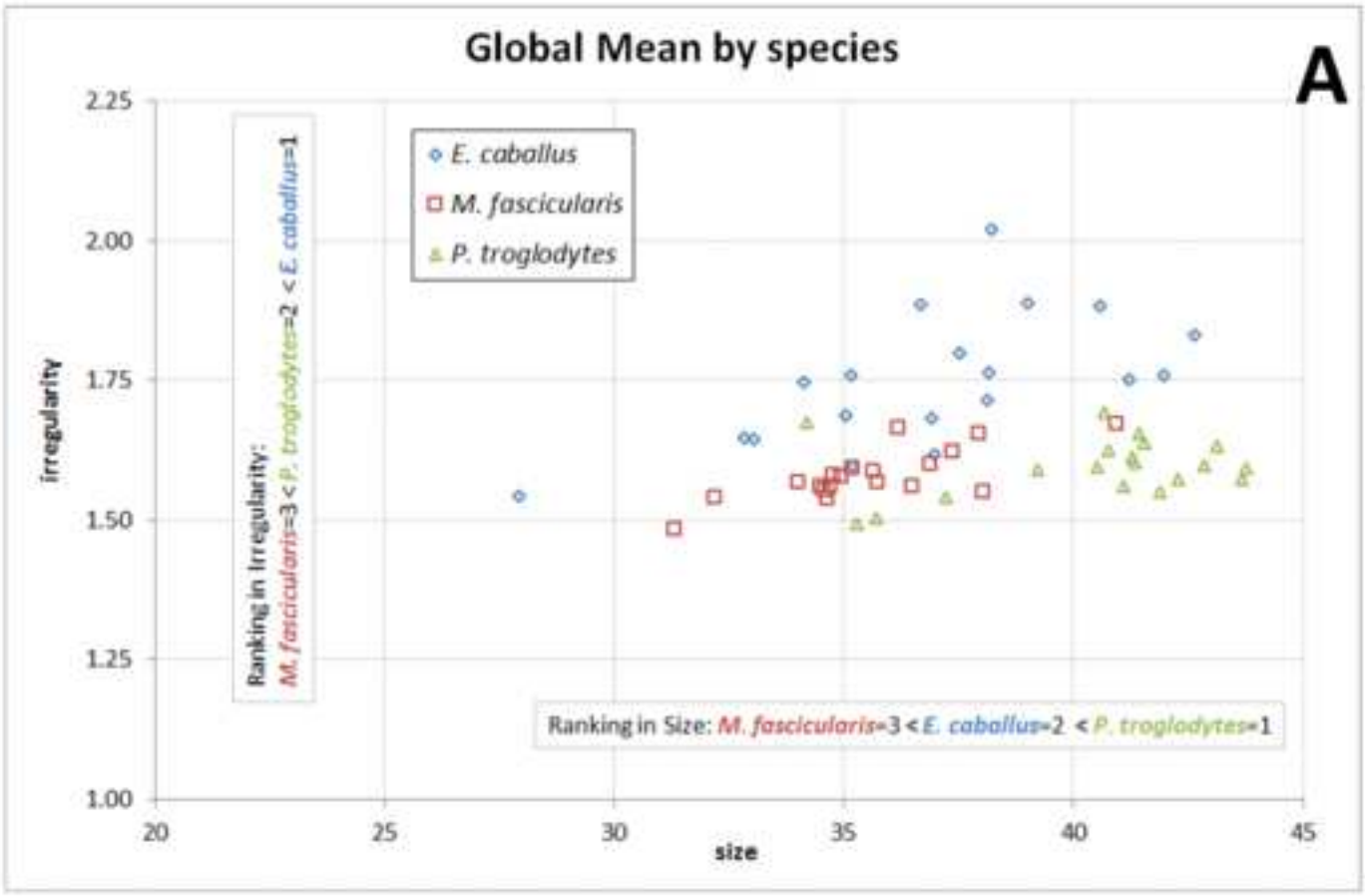
Global Mean by species
A
irregularity
size
E. caballus
M. fascicularis
P. troglodytes
Ranking in Irregularity:
M. fascicularis=3 < P. troglodytes=2 < E. caballus=1
Ranking in Size: M. fascicularis=3 < E. caballus=2 < P. troglodytes=1

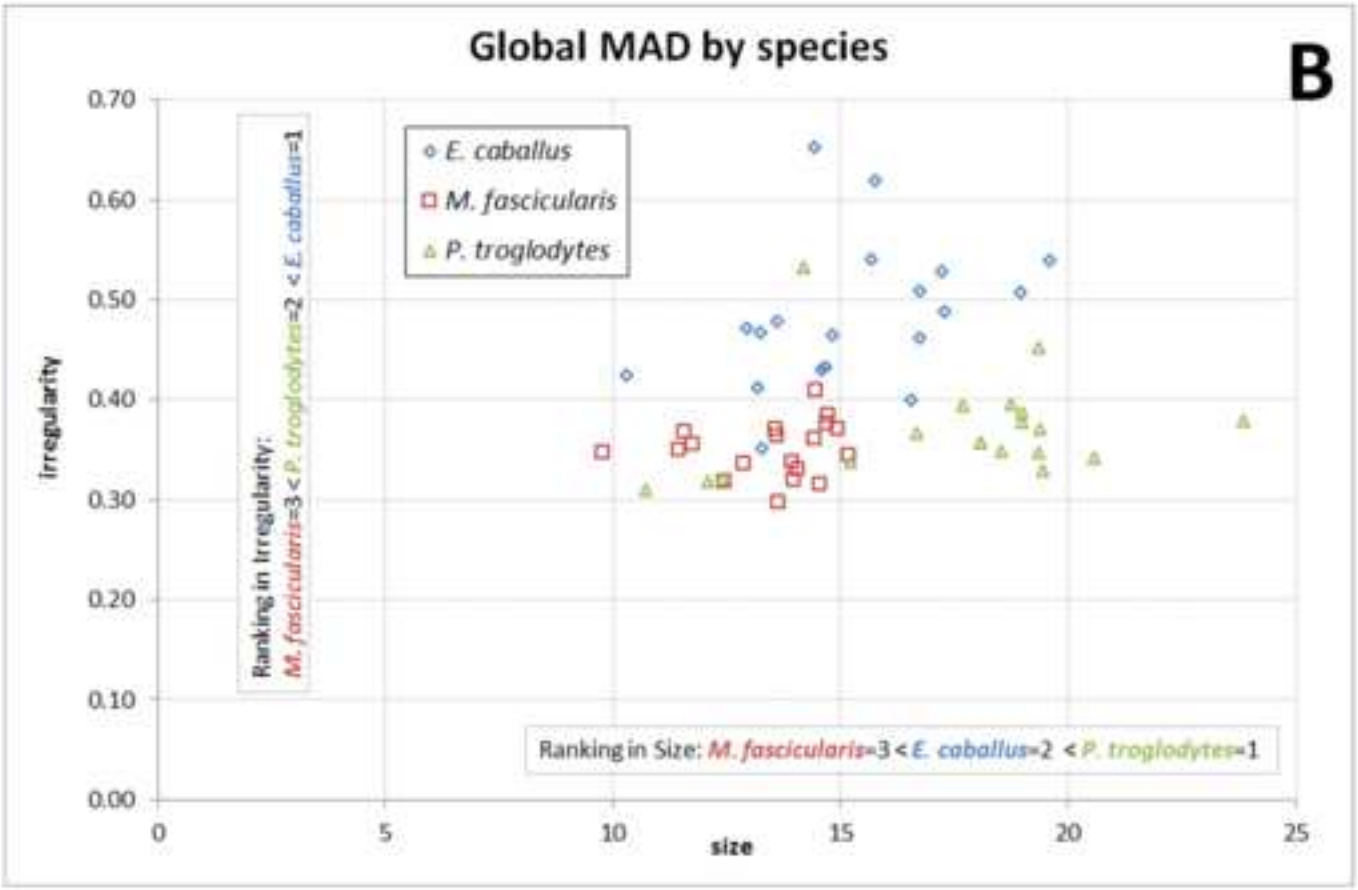
Global MAD by species
B
irregularity
size
E. caballus
M. fascicularis
P. troglodytes
Ranking in Irregularity:
M. fascicularis=3 < P. troglodytes=2 < E. caballus=1
Ranking in Size: M. fascicularis=3 < E. caballus=2 < P. troglodytes=1

Table 1 – List of specimens

species	common name	age	sex	register #	cause of death
Pan troglodytes, Blumenbach, 1775	common chimpanzee	adult	♂	36675	drowning
Pan troglodytes, Blumenbach, 1775	common chimpanzee	25	♂	64361	heart failure
Macaca fascicularis, Raffles, 1821	crab-eating macaque	adult	♀	NHP86	xenotransplant
Macaca fascicularis, Raffles, 1821	crab-eating macaque	adult	♀	NHP86	xenotransplant
Macaca fascicularis, Raffles, 1821	crab-eating macaque	adult	♀	NHP86	xenotransplant
Equus caballus, Linnaeus 1758	domestic horse	adult	♀	not recorded	colic
Equus caballus, Linnaeus 1758	domestic horse	adult	♂	not recorded	heart failure
Equus caballus, Linnaeus 1758	domestic horse	adult	♀	not recorded	colic